Journal of Materials Chemistry A

ROYAL SOCIETY OF CHEMISTRY

PAPER

View Article Online
View Journal | View Issue

Cite this: J. Mater. Chem. A, 2023, 11, 25316

Nitrogen-rich porous organic cages with high acetylene storage and separation performance†

Lijuan Feng,[ab] Yifei Xie,[a] Wenjing Wang,[a] Kongzhao Su *[ac] and Daqiang Yuan *[ac]

Received 14th July 2023
Accepted 19th September 2023

DOI: 10.1039/d3ta04154a

rsc.li/materials-a

Searching for porous materials that can safely store and efficiently separate acetylene (C_2H_2), a commonly used petrochemical feedstock with highly explosive properties, is a pressing and significant task. Nitrogen-rich porous materials have garnered substantial attention for their ability to interact strongly with acidic C_2H_2. Herein, we report two novel nitrogen-rich porous organic cages (POCs), namely **CPOC-107** and **CPOC-203**, constructed from the same bowl-shaped tetraformylcalix[4]resorcinarene but different nitrogen-rich imidazolium-based diamine synthons. X-ray crystallographic analysis reveals that **CPOC-107** adopts a [2 + 4] lantern-shaped structure, whereas **CPOC-203** takes on a [3 + 6] triangular prism shape. Moreover, the cages exhibit large cavity volumes of up to 787 Å^3 and high specific surface areas of up to 1202 m^2 g^{-1}. Owing to their high surface areas and high nitrogen content, both cages exhibit impressive C_2H_2 adsorption capabilities. Specifically, **CPOC-107** achieves a remarkable C_2H_2 uptake value of up to 146 cm^3 g^{-1} at 298 K and 1 atm, the highest among those reported for all porous organic materials to date. Moreover, experimental breakthrough tests have confirmed the effective separation of C_2H_2/CO_2 mixtures using the **CPOC-107** adsorbent.

Introduction

Acetylene (C_2H_2) is a crucial petrochemical material used in the production of industrial products involving polyurethane, polyester plastics, synthetic rubber, and so on.[1,2] However, storing C_2H_2 safely remains challenging due to its flammability and explosive nature when subjected to pressures above 2 atm at room temperature.[3] Moreover, C_2H_2 is usually produced from fractionation and oil cracking, which always involve a small amount of carbon dioxide (CO_2). Therefore, the discrimination of CO_2 to afford high-purity C_2H_2 is critical to high-level safety for various industrial applications.[4] Traditional methods to separate C_2H_2/CO_2 mixtures, such as solvent extraction and cryogenic distillations, not only suffer from high energy-consuming and environment-unfriendly problems but also possess the risk of introducing secondary by-products. Consequently, it is of great importance and urgency to seek better materials for safer storage of C_2H_2 and high-efficiency and low-energy technologies to realize C_2H_2/CO_2 separation.

In recent years, adsorption and separation technologies based on porous materials have shown promise in addressing C_2H_2 storage and separation problems.[5–7] In this region, porous metal–organic frameworks (MOFs) have rapidly developed.[8,9] For instances, **FJI-H8** and **SNNU-98**, reported by Hong and Zhai groups, respectively, have realized gravimetric C_2H_2 uptake values more than 220 cm^3 g^{-1} under ambient conditions.[10,11] Furthermore, **SNNU-45**, a MOF prepared by the Zhai group, has demonstrated the separation of C_2H_2/CO_2 with breakthrough time up to 80 min g^{-1}.[12] In contrast, the development of porous organic materials (POMs) for C_2H_2 storage and separation is markedly slower than that of MOFs. To the best of our knowledge, POMs' C_2H_2 uptake values are generally less than 100 m^2 g^{-1} under ambient conditions, and their ability to separate C_2H_2/CO_2 mixtures *via* actual breakthrough experiments is also underexplored.[13] Therefore, it is crucial to increase their C_2H_2 adsorption capacity and explore their C_2H_2 purification ability to promote the development of POMs in this field.

Porous organic cages (POCs) are an emerging class of low-density crystalline POMs, which are held together from discrete (zero-dimensional; 0D) covalent-bonded macromolecules with permanent intrinsic cavities (0D framework) *via* weak intermolecular interactions.[14–16] Since their inception in 2009 from Cooper's group,[17] research on the design and synthesis of different linkages, shapes, topologies, sizes, and functions of POCs has attracted much attention from chemists and materials scientists.[18–33] Our group focuses on using concave-shaped calix[4]resorcinarene (C4RA) as synthons in construction of

[a]State Key Laboratory of Structural Chemistry, Fujian Institute of Research on the Structure of Matter, Chinese Academy of Sciences, Fuzhou, 350002, China. E-mail: skz@fjirsm.ac.cn; ydq@fjirsm.ac.cn

[b]College of Chemistry, Fuzhou University, Fuzhou, 350116, China

[c]University of the Chinese Academy of Sciences, Beijing, 100049, China

† Electronic supplementary information (ESI) available. CCDC 2255900 and 2255901. For ESI and crystallographic data in CIF or other electronic format see DOI: https://doi.org/10.1039/d3ta04154a

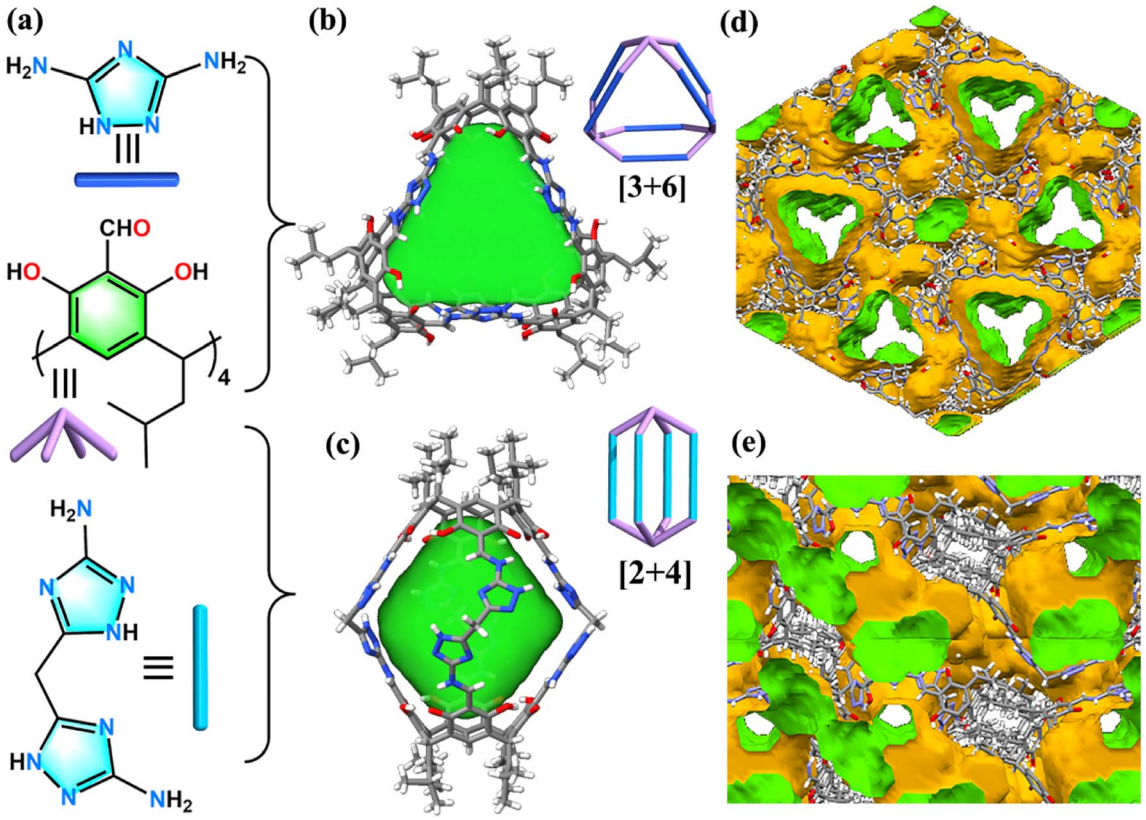

Fig. 1 (a) The chemical structures of organic synthons used for the construction of (b) [3 + 6] **CPOC-203** and (c) [2 + 4] **CPOC-107** obtained from single-crystal X-ray diffraction and the molecular packing for (d) **CPOC-203** and (e) **CPOC-107** in the solid state created with Mercury (voids and contact surface in the crystal shown in green and orange, respectively). Carbon is gold, oxygen red, nitrogen blue, and hydrogen white.

novel C4RA-based POCs and their applications.[34–40] In this work, we designed and synthesized two robust nitrogen-rich POCs aiming at efficient storage and separation of C_2H_2, as the basic nitrogen groups have been verified to have strong interaction with acidic C_2H_2 gas. Both the [2 + 4] lantern-shaped cage (**CPOC-107**) and [3 + 6] triangular prism-shaped cage (**CPOC-203**) are constructed from the same bowl-shaped tetraformylcalix[4]resorcinarene (C4RACHO) but different nitrogen-rich imidazolium-based diamine synthons (Fig. 1a–c and S1–S7†). We found that both materials show high C_2H_2 uptake capacity under ambient conditions (>110 cm^3 g^{-1}), and the nitrogen content greatly influences their C_2H_2 uptake capacity and C_2H_2/CO_2 separation ability.

Results and discussion

A mixture of C4RACHO and 3,5-diamino-1,2,4-triazole (DTA) organic synthons with a molar ratio of 1 : 2 in chlorobenzene and methanol mixture at 80 °C for 24 hours affords red block crystals of **CPOC-203**. Single crystallographic X-ray determination (SCXRD) suggests that **CPOC-203** adopts a triangular prism-shaped cage structure (Fig. 1b), with a [3 + 6] assembly mode that is similar to the previously reported **CPOC-201**, constructed from C4RACHO and *m*-phenylenediamine synthons. **CPOC-203** crystallizes in the triclinic system with the space group $P\bar{1}$ with $Z = 2$, and its asymmetric unit contains one full cage molecule as well as a large number of disordered solvate molecules (~46.2% of the unit cell volume), which have been removed by the routine SQUEEZE function of PLATON.[41] The central triangular prism core of **CPOC-203** comprises three C4RACHO faces and six DTA edges. It has a volume of 787 $Å^3$ and a window diameter of 7.04 Å, as calculated using Voidoo and Pywindow, respectively.[42–44] The cages pack window-to-window in the solid state with the closest distance of ~9 Å between neighboring prism faces, forming one-dimensional channels (Fig. 1d).

Then we further increase the nitrogen content in imidazolium-based diamine synthons by using bis(5-amino-1,2,4-triazol-3-yl)methane (BATM). Notably, suitable red block single crystals of **CPOC-107** can be obtained by an eightfold Schiff base reaction of C4RACHO (1 equiv.) and BATM (2 equiv.) in dimethyl sulfoxide at 100 °C for 72 hours. SCXRD reveals that **CPOC-107** crystallizes in a triclinic $P\bar{1}$ space group with $Z = 4$, and contains a whole [2 + 4] organic cage in its asymmetric unit, and residual electron density as highly disordered solvent molecules (~45.3% of the unit cell volume), which were removed by SQUEEZE. The structure of **CPOC-107** is s a lantern-shaped structure with four near rhombic windows (Fig. 1c), featuring two C4RACHO as faces and four BATMs as pillars. The height of the cavity is 15.4 Å which was measured from the center of the C4RACHO face, and its windows can be passed by a sphere with a diameter of about 4.47 Å. Remarkably, **CPOC-**

107 has a cavity volume of about 744 Å^3, the largest among those of all previously reported lantern-shaped CPOCs, with cavity volumes ranging from 358 to 581 Å^3.[36] The side length of the rhombic windows is about 4.47 Å, which can be passed by a sphere with a diameter of about 4.47 Å. An examination of the **CPOC-107**'s solid-state packing suggested that cage molecules pack *via* weak van der Waals interactions, and there is also a one-dimensional channel in window-to-window mode (Fig. 1e).

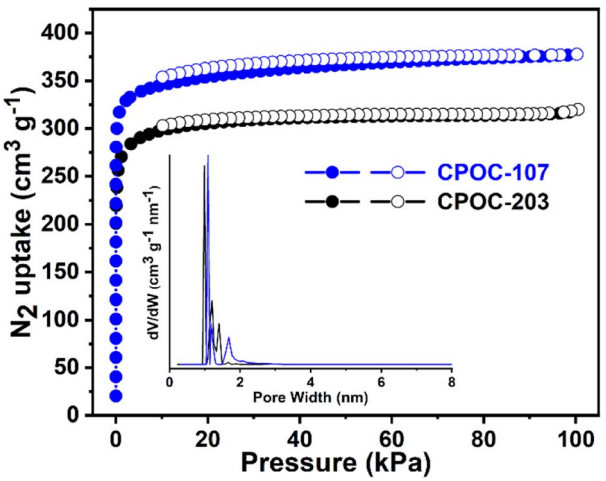

Fig. 2 N_2 gas sorption isotherms at 77 K for **CPOC-107** and **CPOC-203**, inset: the calculated PSD of **CPOC-107** and **CPOC-203**.

The presence of 1D channels in **CPOC-107** and **CPOC-203** prompts us to study their porosity. Thermal gravimetric analysis measurements showed their stabilities up to about 280 °C (Fig. S7†). Before the gas sorption test, both cages are immersed and exchanged 6 times every 24 hours in MeOH before activating at 100 °C under a high vacuum for 12 hours. Powder X-ray diffraction reveals that after desolvation, no phase change occurs in both materials (Fig. S8 and S9†). N_2 gas sorption experiments confirmed their permanent porosity at 77 K (Fig. 2), and both the isotherms of **CPOC-107** and **CPOC-203** exhibited typical type I adsorption behavior with sharp increases at a pressure below 0.1 P/P_o, which reveals their microporous nature. The Brunauer–Emmett–Teller (BET) specific surface areas were 1202 m^2 g^{-1} for **CPOC-107** and 1132 m^2 g^{-1} for **CPOC-203**, respectively (Fig. S10 and S11†). The non-local density functional theory (NLDFT) was used to calculate the pore-size distribution (PSD), and both cages showed microporous cavities with ~1.08 nm for **CPOC-107** and ~0.98 nm for **CPOC-203** (inset in Fig. 2), which are respectively related to the calculated largest pore diameter of 0.94 and 1.02 nm using Zeo++ software.[45]

The high surface, together with the presence of a high content of basic nitrogen sites (14.8% for **CPOC-203** and 20.1% for **CPOC-107**) for both cages, further prompts us to use them as solid adsorbents for capturing acidic C_2H_2 gas and separating C_2H_2/CO_2 mixtures. Single-component gas equilibrium sorption isotherms of **CPOC-107** and **CPOC-203** were recorded at 298 K and pressure up to 1 bar. As shown in Fig. 3a, the saturated

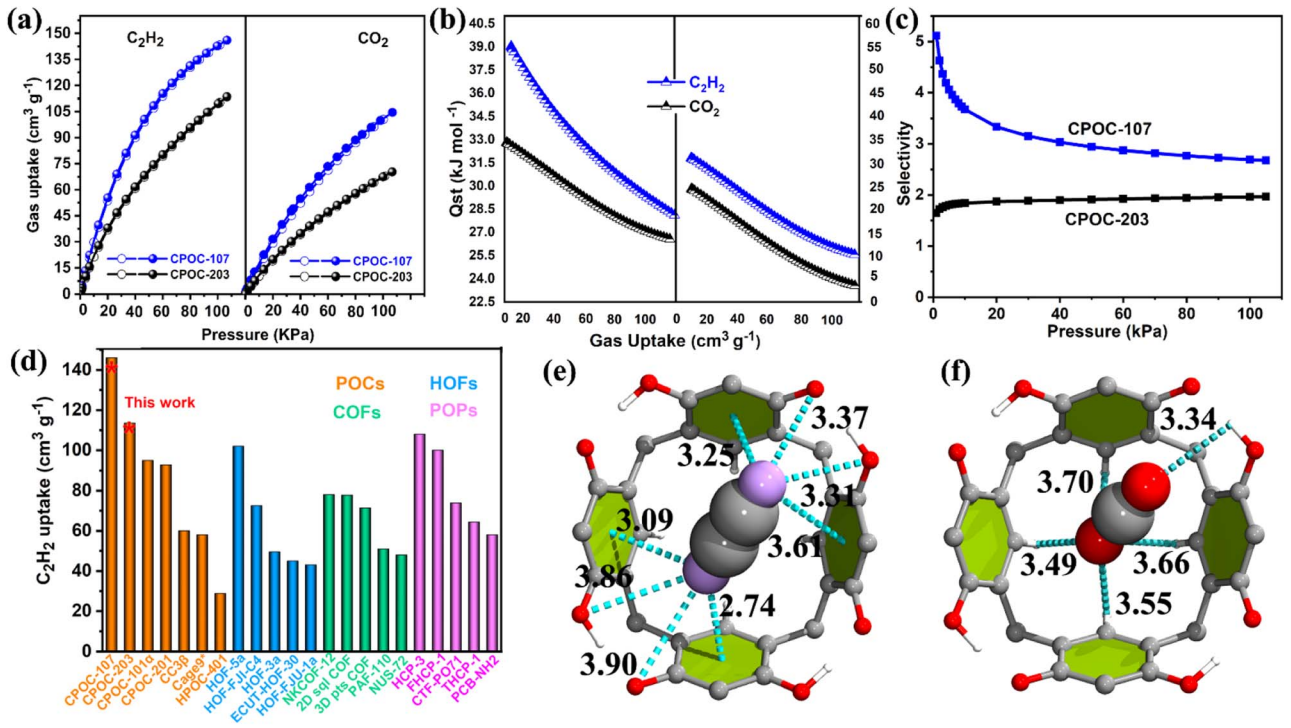

Fig. 3 (a) C_2H_2 and CO_2 sorption isotherms at 298 K; (b) Q_{st} values of C_2H_2 and CO_2; (c) the C_2H_2/CO_2 IAST selectivity; (d) comparison of C_2H_2 uptakes with different top-performed POM adsorbents under ambient conditions; (e) C_2H_2 and (f) CO_2 adsorption sites in **CPOC-107** performed in order to understand its C_2H_2/CO_2 separation mechanism. Carbon is gray, oxygen red, and hydrogen lavender. Dashed bonds highlight H···π and H···O interactions.

C_2H_2 adsorption value under the conditions above is 146 $cm^3 g^{-1}$ for **CPOC-107**, which is higher than that of **CPOC-203**, with a value of 114 $cm^3 g^{-1}$. Both values are higher than those of our previously reported cages with similar structural assemblies. Specifically, the C_2H_2 uptakes for the previously reported lantern-shaped [2 + 4] **CPOC-101** to **CPOC-104** (nitrogen content < 6.2%) are all less than 95 $cm^3 g^{-1}$;[38,46] while for the reported similar triangular prism-shaped [3 + 6] **CPOC-201** with a nitrogen content of 5.8% the C_2H_2 uptake is only 91 $cm^3 g^{-1}$.[38] The discussions above reveal that increasing the nitrogen content in CPOCs can improve their C_2H_2 uptake ability. Notably, the C_2H_2 uptake value (146 $cm^3 g^{-1}$) of **CPOC-107** is the highest among those reported for all POMs (Fig. 3d), including POCs,[47,48] hydrogen-bonded organic frameworks (HOFs),[49–52] covalent organic frameworks (COFs)[53–56] and porous organic polymers (POPs).[57–59]

In contrast, under the same conditions, the CO_2 absorbed capacities of **CPOC-107** and **CPOC-203** are only 100 and 70 $cm^3 g^{-1}$ (Fig. 3a), much lower than their C_2H_2 uptake capacities under the same conditions. Such a result reveals that the affinity for C_2H_2 is stronger than that for CO_2 in both cages. In order to quantify the affinity (low-coverage heat of adsorption; Q_{st}) between the cage hosts and the guest gas molecules, their C_2H_2 and CO_2 sorption isotherms at 273 K have also been measured (Fig. S12†). The Q_{st} values are calculated using adsorption isotherms at 273 and 298 K and fitted by a virial equation (Fig. S13–S16†). The calculated Q_{st} values for C_2H_2 were 39.1 and 34.9 kJ mol^{-1} for **CPOC-107** and **CPOC-203**, respectively, which are higher than those for CO_2 with values of 32.8 and 23.2 kJ mol^{-1}, respectively (Fig. 3b). Such calculated results highly indicate the preferential sorption of C_2H_2 over CO_2 in both cages. Moreover, their gas selectivity values have been calculated using the widely studied ideal adsorbed solution theory (IAST), and the equimolar binary C_2H_2/CO_2 for **CPOC-107** is 2.7 at 298 K and 100 kPa, which is much higher than 1.9 for **CPOC-203**. Moreover, the higher C_2H_2 capacity and C_2H_2/CO_2 selectivity of **CPOC-107** suggest that its separation ability for C_2H_2/CO_2 may be better than that of **CPOC-203**. Therefore, their separation potentials (Δq) are a comprehensive index to evaluate the separation effectiveness of adsorbents based on combining adsorption capacity and selectivity. The calculated Δq value for **CPOC-107** is 2.67 mmol g^{-1}, and for **CPOC-203** it is 1.30 mmol g^{-1} (Fig. S17†), consistent with our guess.[60]

Moreover, the detailed dispersion-corrected density functional theory (DFT-D) calculations for **CPOC-107** were also carried out by loading CO_2 and C_2H_2 molecules into its crystal structure for further optimization. The lowest-energy binding configurations of the final gas-loaded structures of **CPOC-107** were calculated using DFT-D. In the gas-loaded **CPOC-107**, both C_2H_2 and CO_2 molecules were observed to preferentially reside around C4RA's cavities *via* weak Waals interactions (Fig. 3e and f). Specifically, for the C_2H_2 molecule, both hydrogen atoms were oriented toward the four C4RA's phenyl rings through H···π interactions at distances ranging from 2.74 to 3.61 Å. In contrast, their two hydrogen tails were observed to interact with the four C4RA's hydroxy groups through H···O interactions at distances ranging from 3.31 to 3.90 Å. For the CO_2 molecule, one oxygen atom remained closer to the cage's window through O···H interactions at a distance of 3.34 Å. At the same time, the other one was oriented towards the bottom of C4RA through O···H interactions at distances ranging from 3.49 to 3.70 Å. The calculated static binding energies of C_2H_2 and CO_2 were −38.9 and −31.1 kJ mol^{-1}, respectively, for **CPOC-107**. These binding energies and the hydrogen-bond number confirmed the stronger host–guest interactions between C_2H_2 and the cage compared to that of CO_2, which is entirely consistent with our experimental observations.

Lab-scale fixed-bed breakthrough experiments have been performed under ambient conditions to make clear the separation performance of C_2H_2/CO_2 by using **CPOC-107** and **CPOC-203** as adsorbents. An equimolar CO_2/C_2H_2 gas mixture typically flowed over a packed column of the activated samples with a total flow of 2 mL min^{-1} at 298 K and 1 bar. As shown in Fig. 4a, CO_2 passed through the packed column first to produce

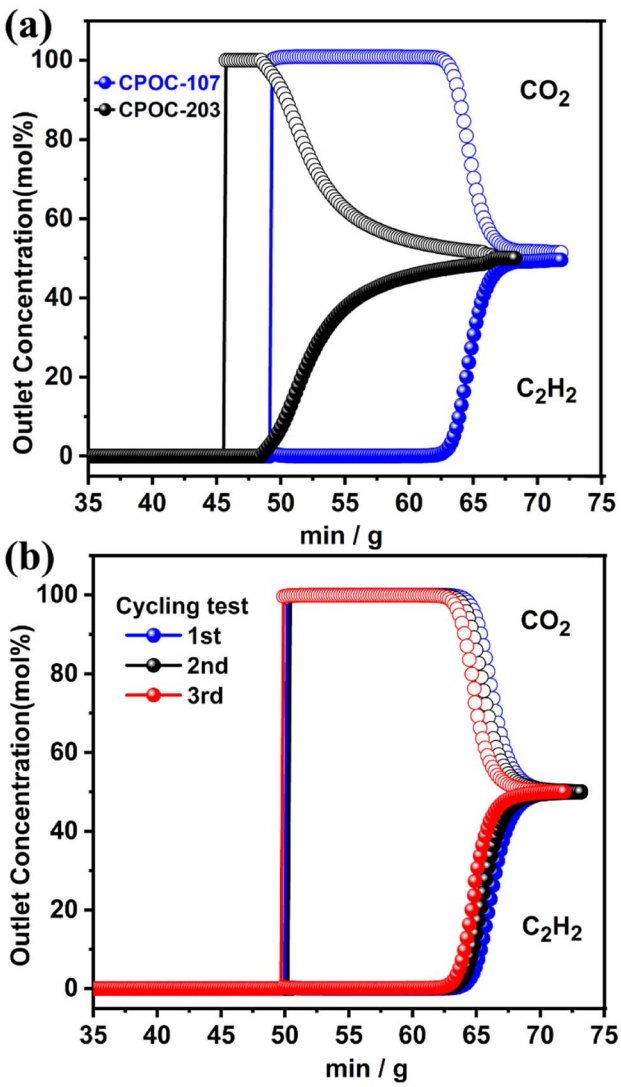

Fig. 4 (a) Experimental breakthrough curves for an equimolar mixture of C_2H_2/CO_2 at 298 K and 1 bar; (b) the recyclability of **CPOC-107** under multiple mixed gas column breakthrough tests.

an outflow of pure gas containing no detectable C_2H_2, and then C_2H_2 eluted following a substantial time-lapse for both CPOC materials. The breakthrough time values of **CPOC-107** and **CPOC-203** are ~13 and 5 min g^{-1}, respectively. The longer effective separation time of **CPOC-107** than **CPOC-203** suggested that the C_2H_2/CO_2 separation ability of **CPOC-107** is better than that of **CPOC-203**, consistent with the above-mentioned IAST and Δq results. An ideal separation material should possess recyclability performance to meet practical applications. To evaluate the durability, multiple cycling breakthrough tests for **CPOC-107** have been carried out under the same conditions. As displayed in Fig. 4b, the breakthrough time remains unchanged after three recycling experiments, indicating that **CPOC-107** is an auspicious C_2H_2/CO_2 separation system.

Conclusions

In summary, we presented two novel C4RA-based POCs with high nitrogen content (>14%), including [2 + 4] lantern-shaped **CPOC-107** and [3 + 6] triangular prism-shaped **CPOC-203**. Both cages exhibit high surface areas (>1100 m^2 g^{-1}), and high C_2H_2 uptake capacity (>110 cm^3 g^{-1}) at 298 K and 1 atm. Notably, the nitrogen content of **CPOC-107** is up to 20.1%, and thus its C_2H_2 uptake capacity under ambient conditions is up to 146 cm^3 g^{-1}, which is the highest among those reported for POMs. Moreover, **CPOC-107** can also efficiently separate C_2H_2/CO_2 with a breakthrough time of 13 min g^{-1}. This work suggests that nitrogen-rich POCs can be promising materials for safer C_2H_2 storage, as well as C_2H_2 purification application. Further studies are focusing on design and synthesis of functionalized POCs by introducing specific group sites for improving their gas storage and separation performances.

Conflicts of interest

There are no conflicts to declare.

Acknowledgements

This work was financially supported by the National Nature Science Foundation of China (22071244 and 22275191), Youth Innovation Promotion Association CAS (2022305), and the Natural Science Foundation of Fujian Province of China (2022J01503 and 2020J05087).

Notes and references

1 V. V. Voronin, M. S. Ledovskaya, A. S. Bogachenkov, K. S. Rodygin and V. P. Ananikov, *Molecules*, 2018, **23**, 2442.
2 P. J. Stang and F. Diederich, *Modern acetylene chemistry*, VCH Weinheim, 1995.
3 R. Matsuda, R. Kitaura, S. Kitagawa, Y. Kubota, R. V. Belosludov, T. C. Kobayashi, H. Sakamoto, T. Chiba, M. Takata, Y. Kawazoe and Y. Mita, *Nature*, 2005, **436**, 238–241.
4 A. Corma, E. Corresa, Y. Mathieu, L. Sauvanaud, S. Al-Bogami, M. S. Al-Ghrami and A. Bourane, *Catal. Sci. Technol.*, 2017, **7**, 12–46.
5 H. Li, C. Liu, C. Chen, Z. Di, D. Yuan, J. Pang, W. Wei, M. Wu and M. Hong, *Angew. Chem., Int. Ed.*, 2021, **60**, 7547–7552.
6 W. Gong, H. Cui, Y. Xie, Y. Li, X. Tang, Y. Liu, Y. Cui and B. Chen, *J. Am. Chem. Soc.*, 2021, **143**, 14869–14876.
7 B. Zhang, Y. Rao, L. Hou, B. Liu and Q. Li, *ACS Mater. Lett.*, 2022, **4**, 1774–1779.
8 Y. Li and G. Wen, *Eur. J. Inorg. Chem.*, 2020, **2020**, 2303–2311.
9 G. Verma, J. Ren, S. Kumar and S. Ma, *Eur. J. Inorg. Chem.*, 2021, **2021**, 4498–4507.
10 J.-W. Wang, S.-C. Fan, H.-P. Li, X. Bu, Y.-Y. Xue and Q.-G. Zhai, *Angew. Chem., Int. Ed.*, 2023, e202217839.
11 J. Pang, F. Jiang, M. Wu, C. Liu, K. Su, W. Lu, D. Yuan and M. Hong, *Nat. Commun.*, 2015, **6**, 7575.
12 Y.-P. Li, Y. Wang, Y.-Y. Xue, H.-P. Li, Q.-G. Zhai, S.-N. Li, Y.-C. Jiang, M.-C. Hu and X. Bu, *Angew. Chem., Int. Ed.*, 2019, **58**, 13590–13595.
13 W. Wang, L. Wang, F. Du, G.-D. Wang, L. Hou, Z. Zhu, B. Liu and Y.-Y. Wang, *Chem. Sci.*, 2023, **14**, 533–539.
14 X. Yang, Z. Ullah, J. F. Stoddart and C. T. Yavuz, *Chem. Rev.*, 2023, 4602–4634.
15 T. Hasell and A. I. Cooper, *Nat. Rev. Mater.*, 2016, **1**, 16053.
16 M. Mastalerz, *Acc. Chem. Res.*, 2018, **51**, 2411–2422.
17 T. Tozawa, J. T. A. Jones, S. I. Swamy, S. Jiang, D. J. Adams, S. Shakespeare, R. Clowes, D. Bradshaw, T. Hasell, S. Y. Chong, C. Tang, S. Thompson, J. Parker, A. Trewin, J. Bacsa, A. M. Z. Slawin, A. Steiner and A. I. Cooper, *Nat. Mater.*, 2009, **8**, 973–978.
18 T. Jiao, H. Qu, L. Tong, X. Cao and H. Li, *Angew. Chem., Int. Ed.*, 2021, **60**, 9852–9858.
19 X. Liu, G. Zhu, D. He, L. Gu, P. Shen, G. Cui, S. Wang, Z. Shi, D. Miyajima, S. Wang and S. Zhang, *CCS Chem.*, 2022, **4**, 2420–2428.
20 S. Huang, Z. Lei, Y. Jin and W. Zhang, *Chem. Sci.*, 2021, **12**, 9591–9606.
21 H. Duan, F. Cao, H. Hao, H. Bian and L. Cao, *ACS Appl. Mater. Interfaces*, 2021, **13**, 16837–16845.
22 S. Bera, K. Dey, T. K. Pal, A. Halder, S. Tothadi, S. Karak, M. Addicoat and R. Banerjee, *Angew. Chem., Int. Ed.*, 2019, **58**, 4243–4247.
23 M. Hua, S. Wang, Y. Gong, J. Wei, Z. Yang and J.-K. Sun, *Angew. Chem., Int. Ed.*, 2021, **60**, 12490–12497.
24 Q.-P. Hu, H. Zhou, T.-Y. Huang, Y.-F. Ao, D.-X. Wang and Q.-Q. Wang, *J. Am. Chem. Soc.*, 2022, **144**, 6180–6184.
25 S. Wu, Y. Ni, Y. Han, S. Xin, X. Hou, J. Zhu, Z. Li and J. Wu, *J. Am. Chem. Soc.*, 2022, **144**, 23158–23167.
26 G. Montà-González, F. Sancenón, R. Martínez-Máñez and V. J. C. R. Martí-Centelles, *Chem. Rev.*, 2022, **122**, 13636–13708.
27 H. Wang, Y. Jin, N. Sun, W. Zhang and J. Jiang, *Chem. Soc. Rev.*, 2021, **50**, 8874–8886.
28 F. Qiu, X. Chen, W. Wang, K. Su and D. Yuan, *CCS Chem.*, 2023, DOI: **10.31635/ccschem.023.202302903**.
29 R. D. Mukhopadhyay, Y. Kim, J. Koo and K. Kim, *Acc. Chem. Res.*, 2018, **51**, 2730–2738.

30 L. Chen, C. Li, E. Fu, M. Li, Y. Kuboi, Z.-Y. Li, Z. Chen, J. Chen, X. Liu, X. Tang, L. Frederic, F. Maurel, C. Adachi, F. Mathevet and S. Zhang, *ACS Mater. Lett.*, 2023, **5**, 1450–1455.
31 W.-T. Dou, C.-Y. Yang, L.-R. Hu, B. Song, T. Jin, P.-P. Jia, X. Ji, F. Zheng, H.-B. Yang and L. Xu, *ACS Mater. Lett.*, 2023, **5**, 1061–1082.
32 M. C. Brand, F. Greenwell, R. Clowes, B. D. Egleston, A. Kai, A. I. Cooper, T. D. Bennett and R. L. Greenaway, *J. Mater. Chem. A*, 2021, **9**, 19807–19816.
33 S. Lee, I. Kevlishvili, H. J. Kulik, H.-T. Kim, Y. G. Chung and D.-Y. Koh, *J. Mater. Chem. A*, 2022, **10**, 24802–24812.
34 F. Gao, C. Luo, X. Wang, C. Zhan, Y. Li, Y. Li, Q. Meng, M. Yang, K. Su, D. Yuan, R. Zhu and Q. Zhao, *Adv. Funct. Mater.*, 2023, **33**, 2211900.
35 N. Xu, K. Su, E.-S. M. El-Sayed, Z. Ju and D. Yuan, *Chem. Sci.*, 2022, **13**, 3582–3588.
36 M. Yang, F. Qiu, E.-S. M. El-Sayed, W. Wang, S. Du, K. Su and D. Yuan, *Chem. Sci.*, 2021, **12**, 13307–13315.
37 X. Zhang, K. Su, A. G. A. Mohamed, C. Liu, Q. Sun, D. Yuan, Y. Wang, W. Xue and Y. Wang, *Energy Environ. Sci.*, 2022, **15**, 780–785.
38 K. Su, W. Wang, S. Du, C. Ji, M. Zhou and D. Yuan, *J. Am. Chem. Soc.*, 2020, **142**, 18060–18072.
39 M. Yang, X. Chen, Y. Xie, E.-S. M. El-Sayed, N. Xu, W. Wang, K. Su and D. Yuan, *Sci. China: Chem.*, 2023, **66**, 1763–1770.
40 K. Su, W. Wang, S. Du, C. Ji and D. Yuan, *Nat. Commun.*, 2021, **12**, 3703.
41 A. L. Spek, *Acta Crystallogr., Sect. C: Struct. Chem.*, 2015, **71**, 9–18.
42 **https://xray.bmc.uu.se/usf/**.
43 G. J. Kleywegt and T. A. Jones, *Acta Crystallogr., Sect. D: Biol. Crystallogr.*, 1994, **50**, 178–185.
44 S. Sanz, K. Ferreira, R. D. McIntosh, S. J. Dalgarno and E. K. Brechin, *Chem. Commun.*, 2011, **47**, 9042–9044.
45 S. M. Taylor, R. D. McIntosh, C. M. Beavers, S. J. Teat, S. Piligkos, S. J. Dalgarno and E. K. Brechin, *Chem. Commun.*, 2011, **47**, 1440–1442.
46 W. Wang, K. Su, E.-S. M. El-Sayed, M. Yang and D. Yuan, *ACS Appl. Mater. Interfaces*, 2021, **13**, 24042–24050.
47 S. M. Elbert, N. I. Regenauer, D. Schindler, W.-S. Zhang, F. Rominger, R. R. Schroeder and M. Mastalerz, *Chem.–Eur. J.*, 2018, **24**, 11438–11443.
48 C. D. Charles and E. D. Bloch, *Supramol. Chem.*, 2019, **31**, 508–513.
49 P. Li, Y. He, Y. Zhao, L. Weng, H. Wang, R. Krishna, H. Wu, W. Zhou, M. O'Keeffe, Y. Han and B. Chen, *Angew. Chem., Int. Ed.*, 2015, **54**, 574–577.
50 H. Wang, B. Li, H. Wu, T.-L. Hu, Z. Yao, W. Zhou, S. Xiang and B. Chen, *J. Am. Chem. Soc.*, 2015, **137**, 9963–9970.
51 Y. Yang, H. Zhang, Z. Yuan, J.-Q. Wang, F. Xiang, L. Chen, F. Wei, S. Xiang, B. Chen and Z. Zhang, *Angew. Chem., Int. Ed.*, 2022, **61**, e202207579.
52 L. Wang, L. Yang, L. Gong, R. Krishna, Z. Gao, Y. Tao, W. Yin, Z. Xu and F. Luo, *Chem. Eng. J.*, 2020, **383**, 123117.
53 L. Chen, C. Gong, X. Wang, F. Dai, M. Huang, X. Wu, C.-Z. Lu and Y. Peng, *J. Am. Chem. Soc.*, 2021, **143**, 10243–10249.
54 L. Jiang, Y. Tian, T. Sun, Y. Zhu, H. Ren, X. Zou, Y. Ma, K. R. Meihaus, J. R. Long and G. Zhu, *J. Am. Chem. Soc.*, 2018, **140**, 15724–15730.
55 Z. Zhang, C. Kang, S. B. Peh, D. Shi, F. Yang, Q. Liu and D. Zhao, *J. Am. Chem. Soc.*, 2022, **144**, 14992–14996.
56 P. Zhang, Z. Wang, Y. Yang, S. Wang, T. Wang, J. Liu, P. Cheng, Y. Chen and Z. Zhang, *Sci. China: Chem.*, 2022, **65**, 1173–1184.
57 S. Zhang, M. K. Taylor, L. Jiang, H. Ren and G. Zhu, *Chem.–Eur. J.*, 2020, **26**, 3205–3221.
58 Z. Jia, J. Pan and D. Yuan, *ChemistryOpen*, 2017, **6**, 554–561.
59 X. Liu, C. Xu, X. Yang, Y. He, Z. Guo and D. Yan, *Microporous Mesoporous Mater.*, 2019, **275**, 95–101.
60 Y. Jiang, J. Hu, L. Wang, W. Sun, N. Xu, R. Krishna, S. Duttwyler, X. Cui, H. Xing and Y. Zhang, *Angew. Chem., Int. Ed.*, 2022, **61**, e202200947.